Journal of Geophysical Research: Oceans

RESEARCH ARTICLE
10.1029/2018JC014226

Key Points:
- The joint effect of tidal mixing and stratification is essential to the upwelling generation west and southwest off the Hainan Island
- With tides included, currents induced by the baroclinic pressure gradient are the main drivers of the cold water uplifting
- The winds, the tides, and the boundary currents are the main causes of upwelling variations, with the winds being the largest contributor

Correspondence to:
S. Peng and H. Huang,
speng@scsio.ac.cn;
mrhuanghu@126.com

Citation:
Li, Y., Peng, S., Wang, J., Yan, J., & Huang, H. (2018). On the mechanism of the generation and interannual variations of the summer upwellings west and southwest off the Hainan Island. *Journal of Geophysical Research: Oceans*, *123*, 8247–8263. https://doi.org/10.1029/2018JC014226

Received 30 MAY 2018
Accepted 20 OCT 2018
Accepted article online 24 OCT 2018
Published online 19 NOV 2018

On the Mechanism of the Generation and Interannual Variations of the Summer Upwellings West and Southwest Off the Hainan Island

Yineng Li[1], Shiqiu Peng[1,2,3], Jia Wang[4], Jing Yan[1], and Hu Huang[3]

[1]State Key Laboratory of Tropical Oceanography, South China Sea Institute of Oceanology, Chinese Academy of Sciences, Guangzhou, China, [2]Laboratory for Regional Oceanography and Numerical Modeling, Qingdao National Laboratory for Marine Science and Technology, Qingdao, China, [3]Guangxi Key Laboratory of Marine Disaster in the Beibu Gulf, Qinzhou University, Qinzhou, China, [4]NOAA Great Lakes Environmental Research Laboratory, Ann Arbor, MI, USA

Abstract The generation and interannual variations of the upwellings west and southwest off the Hainan Island (hereafter denoted as UWHI and USWHI, respectively) detected from satellite-derived sea surface temperature as well as the mechanism behind them are investigated using a 3-D high-resolution ocean model with a set of sensitivity experiments. The model is able to reproduce the upwellings with significant variations in the seasonal and interannual time scales. Results of sensitivity experiments show that the joint effect of tidal mixing and stratification is the main cause of the generation of both UWHI and USWHI in summer, and the offshore pattern of the upwelling centers is closely associated with that of high mixing rate centers where currents interact with steep bathymetry. In addition, the circulation changes induced by the joint effect of tidal mixing and stratification have significant impacts on the upwellings, especially on USWHI. For the interannual variations of both UWHI and USWHI, the changes of the along-shore winds, the tidal mixing, and the boundary currents are the main causes of the variations; the weak tidal mixing, enhanced along-shore winds, and strong boundary currents result in the weakest upwellings there in 1998, with the enhanced along-shore wind being the largest contributor.

Plain Language Summary Based on the numerical results, the joint effect of tidal mixing and stratification is the main cause of the generation of both the upwellings west and southwest off the Hainan Island. In addition, the weak tidal mixing, enhanced along-shore winds, and strong boundary currents result in the weakest upwellings there in 1998, with the enhanced along-shore wind being the largest contributor.

1. Introduction

Upwelling is an important dynamic process in coastal regions. Upwelling lifts cold and nutritious waters from the deeper ocean to the surface and subsurface, facilitating the bloom of phytoplankton and then the growth of fish (Ekman, 1905). The dynamics of upwelling as well as its impacts on marine ecosystems have attracted more and more attentions in the recent decades (e.g. Bakun et al., 2010; Menge & Menge, 2013). Generally, wind-induced Ekman transport and Ekman pumping are considered to be the main drivers of coastal upwelling occurrence, but they differ in different coastal regions (Ekman, 1905).

The coastal upwelling along the Hainan Island, which is located in the northwestern South China Sea (SCS; Figure 1a), has gained considerable attentions, too. There are two main upwelling regions around the Hainan Island, those are, the eastern coast and the western/southwestern coast of the Island. Previous studies are mainly focused on the upwelling east off the Hainan Island, which can be traced back to the 1960s (Guan & Chen, 1964; Niino & Emery, 1961). The strong upwelling east off the Hainan Island usually occurs during June to August due to the steady and strong East Asia Summer Monsoon (Guo et al., 1998; Jing et al., 2009, 2011; Zeng et al., 2014). Using observations and a two-dimensional diagnostic model, Guo et al. (1998) calculated the maximum vertical velocity to be 3.21×10^{-5} m/s at a depth of 30 m, 10 km offshore. The wind-driven Ekman transport and Ekman pumping were suggested to be the main mechanism of the upwelling east off the Hainan Island (Guo et al., 1998; Jing et al., 2009, 2011; Zeng et al., 2014). Moreover, the intensity of the upwelling east off the Hainan Island may vary interannually due to the variation of East Asia Summer Monsoon (Wang et al., 2006) or large-scale circulations (Li et al., 2012; Su et al., 2013).

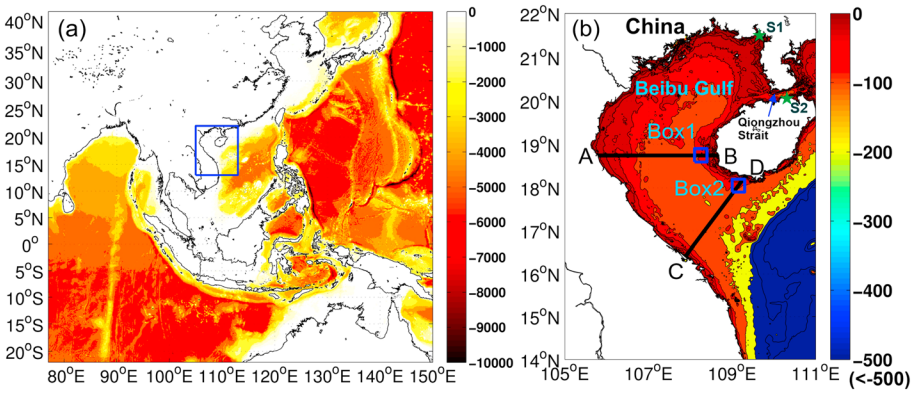

Figure 1. The bathymetry (unit: m) of the (a) outer and inner domains and (b) the region around the UWHI and USWHI (the green stars are the locations of tide gauges, S1 for Beihai and S2 for Haikou). UWHI = upwelling west off the Hainan Island; USWHI = upwelling southwest off the Hainan Island.

In contrast, only a few studies have paid attention on the upwelling west and southwest off the Hainan Island (hereafter denoted as UWHI and USWHI, respectively) in the southeastern part of Beibu Gulf (Lü et al., 2008; Zhang et al., 2010; Wang et al., 2016). The sea surface temperature (SST) in the Beibu Gulf shows large seasonal and spatial variability: In summer, the shallower area in the north of the Beibu Gulf is generally warmer than the deeper area in the south because of bathymetric effect under solar radiation (Su & Yuan, 2005) and the upwelled cold water can appear in the west off the Hainan Island (Chai et al., 2001; Li, 1990); in winter, SST is high in the deep water and low near the coast due to surface cooling and bathymetric effect (Xie et al., 2002). Zhang et al. (2010) also noticed a center of cooler subsurface water southwest off the Hainan Island. Unlike the upwelling along the eastern coast, the local tide-induced mixing is considered to be the main factor producing UWHI (Lü et al., 2008; Wang et al., 2016). In the interannual scale, however, the variations of UWHI and USWHI and their forcing factors have not yet been investigated. Some important issues remain unsolved, which this study aims to address: What are the main factors causing the generation of upwelling (except for the tidal mixing) and the interannual variations of upwelling in the regions west and southwest off the Hainan Island? What are the differences regarding the controlling factors of generation and variations between UWHI and USWHI?

In this paper, satellite remote sensing SST data and model simulation outputs are employed to investigate the generation and interannual variations of UWHI and USWHI as well as the mechanism behind them. The paper is organized as follows. Section 2 gives a description of the satellite data, model configuration, and validation. The surface features and variations of the upwelling from satellite observations and model outputs are shown in section 3. Section 4 presents the results of sensitive experiments and dynamical analysis regarding the main factors affecting the variations of UWHI and USWHI. A conclusion is given in section 5.

2. Data and Methodology

2.1. Satellite Data

The satellite data used in this study include SST reanalysis with 4-km resolution from the Advanced Very High Resolution Radiometer (AVHRR) and daily-averaged Moderate Resolution Imaging Spectroradiometer (MODIS)_Aqua level 3 data with 4-km resolution. The MODIS data are provided by the Jet Propulsion Laboratory (JPL) of National Aeronautics and Space Administration (NASA), which captures data in 36 spectral bands ranging in wavelength from 0.4 to 14.4 μm and at varying spatial resolutions (2 bands at 250 m, 5 bands at 500 m, and 29 bands at 1 km).

2.2. Model Description and Configuration

The 2004 version of the POM (Blumberg & Mellor, 1987; Mellor, 2004) is employed in this study. The POM is a 3-D, fully nonlinear, primitive equation ocean model, with the 2.5-order turbulence closure scheme of Mellor and Yamada (1982) for calculating turbulence viscosity and diffusivity.

Table 1
The Experimental Design

Experiment	Stratification	BC currents (SSH/U/V)	TIDE	Wind	Objective
CTRL	Yes	Climatology	Included (1998)	Climatology	Control run
EXP1	Yes	Climatology	Not included	Climatology	To investigate the effect of tides
EXP2	No	Climatology	Included (1998)	Climatology	To investigate the effect of stratification
EXP3	Yes	Climatology	Included (2003)	Climatology	To investigate the effect of tide variation
EXP4	Yes	Climatology	Included (1998)	1998	To investigate the effect of wind variation
EXP5	Yes	1998	Included (1998)	Climatology	To investigate the effect of boundary current variation

Note. BC = boundary condition; SSH = sea surface height. U and V denote currents.

A nested-domain configuration is employed as shown in Figure 1. The outer model domain covers the Eastern Indian Ocean, the SCS, and the West Pacific from 22°S to 41.5°N and 77°E to 150°E, with a horizontal resolution of 1/9° (about 12 km) and 35 vertical layers in sigma coordinate refined in both upper and near-bottom ocean. The inner domain envelops the whole Hainan Island as well as the Beibu Gulf in the northwestern SCS from 13°N to 22°N and 105°E to 113°E, with a horizontal resolution of 1/27° (about 4 km). The vertical sigma layers are the same as those in the outer domain. The 1-arcmin global relief model of Earth's topography and bathymetry (Marks & Smith, 2006) is used. For the near-shore region, the model's minimum depth is set to 10 m, based on a physical stability criterion of the global stability by Wang (1996): $h_{\min} + \zeta_{\max} > 0$, where $h_{\min}$ is the minimum water depth and $\zeta_{\max}$ is the maximum water elevation possibly caused by strong (gusty) winds along the coast. The external and internal time steps are set to 6 and 240 s, respectively. Monthly-mean data from the Simple Ocean Data Assimilation (SODA3.3.1) reanalysis (Carton & Giese, 2008) are used for the open boundaries of the outer domain. The normal advection of different variables at the open boundaries is governed by the radiation boundary condition (Mellor, 2004).

The initialization procedure of the ocean model includes two steps. First, the POM is integrated from a rest state of the ocean (i.e., "cold start"). The initial temperature and salinity are from the climatological fields of the World Ocean Atlas 2013 for January (Locarnini et al., 2013), and the 6-hourly climatological wind stress, heat flux, and shortwave radiation flux are from the National Center for Atmospheric Research/National Center of Environment Prediction reanalysis (Kalnay et al., 1996). After a 20-year spin-up of the model, the upper ocean can reach a quasi-equilibrium state (Zhang & Qian, 1999). The second step is to integrate the POM from 1 January 1987 to 31 December 2010, while the outputs from 1988 are used for analysis. The 6-hourly meteorological forcing data, including sea surface winds, air temperature, humidity, E-P (evaporation minus precipitation) and shortwave radiation flux are obtained from the National Center of Environment Prediction/ National Center for Atmospheric Research reanalysis as well. For the inner domain, two 24-year model runs with and without tidal forcing in the boundary are implemented, which are denoted as TIDE and NOTIDE. The tides are incorporated into the inner model through the open boundaries with 13 tidal constituents from the OTPS (Oregon State University Tidal Prediction Software; Egbert et al., 1994).

2.3. Experimental Design

To investigate the joint effect of tidal mixing and the seasonal background stratification, as well as how tides, winds, and boundary currents affect the interannual variations of UWHI and USWHI, a set of experiments is designed for the inner model in this study, as given in Table 1. It should be noted that the "background stratification" mentioned here is referred to the seasonal stratification without tidal effect, which is mainly induced by the variation of surface forcing and lateral boundary conditions. The tides, winds, and boundary currents in 1998 or 2003 are selected to replace the climatology respectively for each sensitivity experiment. Here the summer of 1998, which follows the winter of 1997 with strong El Niño-Southern Oscillation, is featured with the weakest vertical velocity, bottom mixing rate, and strong along-shore wind and boundary currents, while the summer of 2003 has a very strong bottom mixing rate as shown in Figure 2. CTRL is the one-year standard model run with the boundary conditions and surface forcing from climatology and tidal forcing of 1998. EXP1 is similar to CTRL except that tidal effect is not included, which investigates the impact of tidal mixing on UWHI and USWHI by comparing to CTRL. EXP2 is similar to CTRL except that stratification is removed (temperature is fixed to 25 and salinity is fixed to 34 in all grids). The rest of the experiments (EXP3 to EXP5) are designed to further investigate how the variations of tidal forcing, surface wind forcing, and lateral

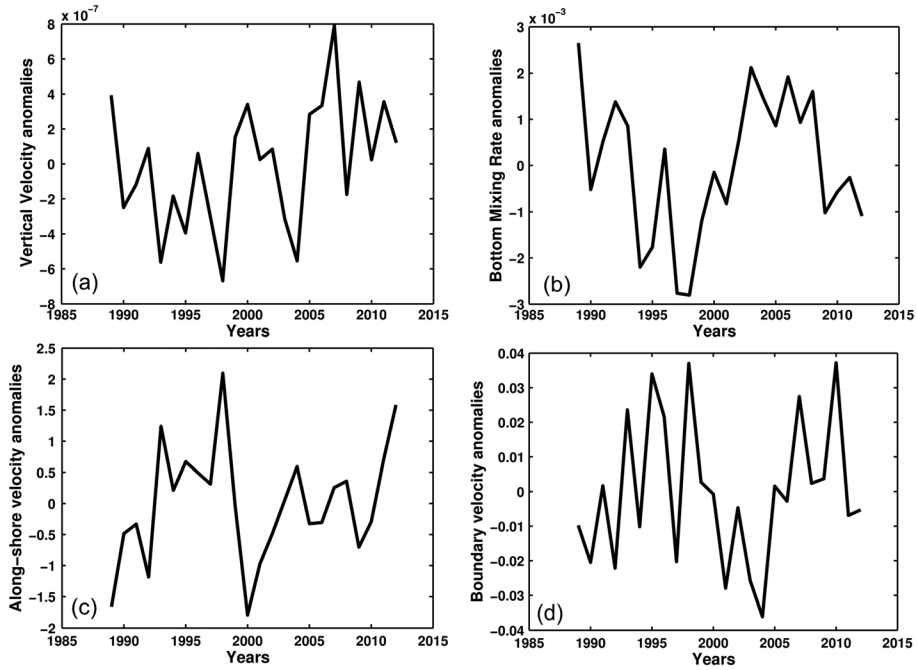

Figure 2. The interannual variations of (a) the vertical velocity anomalies (unit: m/s), (b) the mixing rate anomalies in the bottom ocean (unit: 10^{-3} m^2/s), (c) the along-shore wind speed anomalies (unit: m/s) averaged over Box 1 (referred to in Figure 1b), and (d) the vertical-averaged current anomalies along the south boundary (unit: m/s) in July. (The anomalies are calculated by subtracting the climatological monthly mean of July during 1988 to 2010 from the monthly mean of July in specific years. The vertical velocity, the mixing rate, and vertical-averaged current are directly extracted from the model outputs during the forward integration. Here the mixing rate is from the outputs of vertical diffusivity [KH] in the model. The details of the KH calculation can be found in the manual of POM model; Mellor, 2004.)

currents affect UWHI and USWHI. EXP3 is similar to CTRL except that the tidal forcing of 1998 is changed to that of 2003. EXP4 (EXP5) is similar to CTRL except that EXP4 (EXP5) changes the surface wind forcing (lateral boundary sea surface height [SSH] and currents) from climatology to 1998. All the experiments start from the first day of the simulating year and share the same Initial Conditions (ICs) which are obtained after 20 year's spin-up.

2.4. The Model Validation

To ensure the modeled results are reliable, a quick model validation is made here, which focuses on the circulation, tides, and SST. The traditional understanding of the currents in the Beibu Gulf suggested by Yu and Liu (1993) is that a cyclonic circulation occurs in winter and the circulation pattern reverses in summer. Recent studies show that the circulations are weak and still cyclonic in summer (e.g., Bao et al., 2005; Wu et al., 2008; Xia et al., 2001). Figures 3a–3d show that a weak and cyclonic circulation inside the Beibu Gulf occurs in spring and summer, while strong cyclonic circulation occurs in autumn and winter. Moreover, the observation results from Shi et al. (2002) show that the flow in the Qiongzhou Strait is year-round westward and the transport is around 0.2–0.4 Sv during winter and spring and 0.1–0.2 Sv during summer and autumn. Figure 4 shows a similar trend of transport in the Qiongzhou Strait. These results indicate that the model can provide a reasonable circulation in the Beibu Gulf. For the tidal simulation, it is validated against tidal observations from two tide gauge stations (Beihai and Haikou shown in Figure 1b) from the research quality data set of Joint Archive for Sea Level, which is provided by the University of Hawaii Sea Level Center. The correlations between the modeled and observed water level reach 0.99 and 0.97 with mean relative errors of 5% and 7% for Beihai and Haikou, respectively. Accounting for the 4-km horizontal resolution in this study and the errors of the bathymetry, the accuracy of tidal simulation is acceptable. SST is one of the key variables for identifying the upwelling phenomena; thus, we validate the modeled SST against the satellite-observed SST to see whether the model can reproduce the upwelling process in the coastal regions. Here we use the monthly-mean SST from AVHRR and MODIS_Aqua, which were created using daily data from 1985 to 2010 and

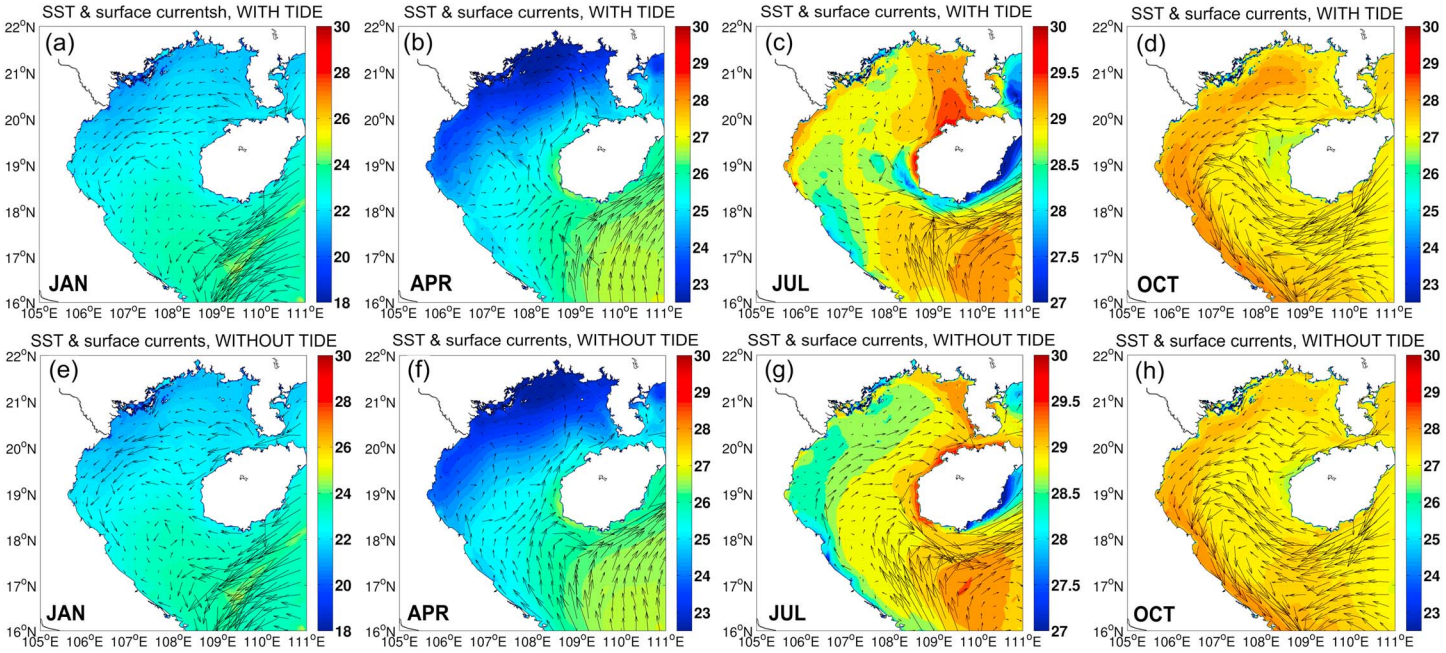

Figure 3. The sea temperatures (unit: °C) superimposed by surface currents of the inner-domain model for experiments (top) TIDE and (bottom) NOTIDE in (a, e) January, (b, f) April, (c, g) July, and (d, h) October. SST = sea surface temperature.

from 2003 to 2015, respectively. The results shown in Figures 3 and 5 indicate that the model can reproduce the seasonal variation of SST as well as the centers of cold surface water in the regions west and southwest off the Hainan Island when tides are included in the model. Therefore, the model results are reliable to be used for investigating the generation and interannual variations of UWHI and USWHI as well as the mechanism behind them.

3. The Features and Variations of UWHI and USWHI

3.1. The Features of the Summer Upwelling

The climatological monthly-mean SST from July (Figures 5c and 5g) shows that the cooler surface water centers can be observed west and southwest off the Hainan Island as well as east and northeast. From winter to spring (January and April shown in Figure 5), no significant cooler surface water centers can be seen around the Hainan Island in both two satellite data sets. In July, the strong southwesterly winds are prevalent (Figure 5k), which induces strong upwelling east off the Hainan Island through Ekman transport and Ekman pumping (Figures 5c and 5g; Jing et al., 2009, 2011). However, these strong southwesterly winds induce downwelling or suppress upwelling west off the Hainan Island. In October, the cooler sea surface temperature east off the Hainan Island disappears in the wake of the reversing winds from southwesterly to northeasterly (Figure 5l), indicating that the upwelling is weaken there. These results reveal that in most of the summertime the winds are favorable to induce the upwelling east off the Hainan Island, whereas they suppress the upwelling west off the Island.

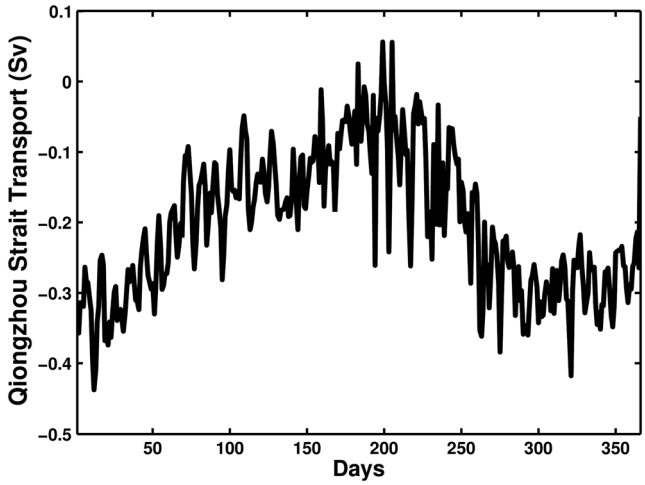

Figure 4. The daily variation of Qiongzhou Strait transport (unit: Sv).

Consequently, the mechanism for UWHI or USWHI should be different with the upwelling east off the Island. As discussed in Lü et al. (2008), the tide-induced mixing is the dynamic source of UWHI. The tidal effect can be seen in the SST of the inner domain (Figures 3c and 3g). When tides are excluded, however, the cooler sea surface water centers vanish, indicating that tidal effect is the essential factor for the generation of UWHI and

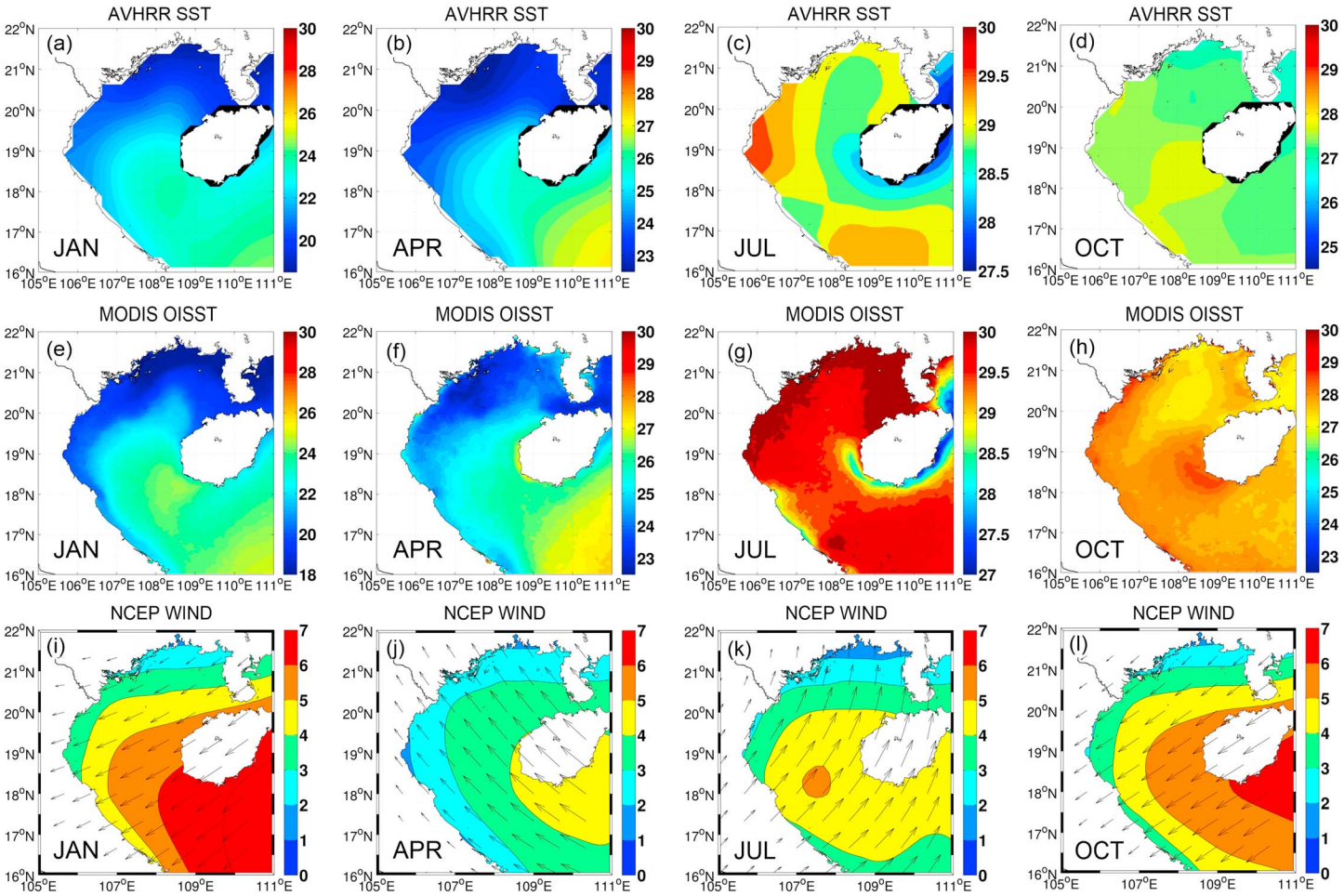

Figure 5. The climatological monthly-mean (top) NOAA AVHRR SSTs (unit: °C), (middle) MODIS_Aqua (unit: °C), (bottom) wind speed and direction (unit: m/s) from NCEP analysis around the Hainan Island in (a, e, i) January, (b, f, j) April, (c, g, k) July, and (d, h, l) October. NOAA = National Oceanic and Atmospheric Administration; AVHRR = Advanced Very High Resolution Radiometer; SST = sea surface temperature; MODIS = Moderate Resolution Imaging Spectroradiometer; NCEP = National Center of Environment Prediction.

USWHI. For the seasonal variation, as shown in Figure 6, the SST drops dramatically compared to that from the NOTIDE when strong upwelling (positive vertical velocity) occurs in both regions of UWHI and USWHI in summer. In cold seasons, although the upwelling is strong in the region west off the Hainan Island (Figure 6a), which is mainly caused by the strong northeasterly winds, the differences of SST are slim between TIDE and NOTIDE (Figure 6b) due to the well-mixed water in the upper layers. Therefore, it should be noted that UWHI exists in both warm and cold seasons, but its appearance in SST is different for the two seasons; the effect of winds is also different on UWHI for the two seasons, that is, the northeasterly winds in winter favor UWHI, whereas the southwesterly winds in summer suppress UWHI, implying that UWHI in summer may be driven by other factors except for winds. In this study, we thus focus on the generation and variations of the upwellings west and southwest off the Hainan Island in summer.

3.2. Interannual Variations of UWHI and USWHI

To investigate the interannual variations of the upwelling, the area-averaged SST anomalies of the two regions (Box 1/Box 2 shown in Figure 1b) against the whole inner-domain model are analyzed. As shown in Figure 7, significant interannual variations can be found in both modeled and satellite-derived SSTs. The standard deviations of the modeled SST west (southwest) off the Hainan Island in the annual scale are around 0.29 °C(0.30 °C), while those from the satellite are 0.30 °C (0.32 °C). Please be aware that the modeled SST is the sea temperature in the first layer of the model, which is not the real surface skin temperature as

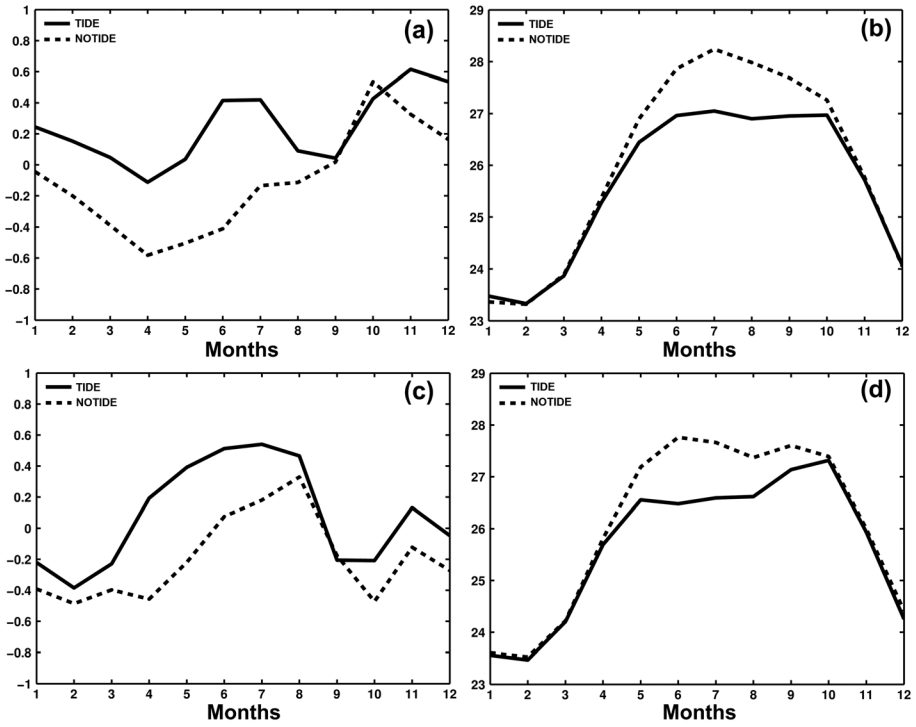

Figure 6. The monthly variations of (left) modeled vertical velocities (unit: 10^{-5} m/s) and (right) sea surface temperature (unit: °C) from inner-domain model outputs (dotted lines for NOTIDE; black lines for TIDE) averaged over (a and b) Box 1 and (c and d) Box 2, which are indicated in Figure 1b.

measured by satellites. It is obvious that when tides are excluded in the model, the modeled SST has much larger biases, especially for the western coast (Box 1). However, the correlation coefficient of SST between model outputs and satellite data for the interannual variations has only a marginal change, from 0.62 to 0.58 (0.65 to 0.64) for Box 1 (Box 2). It implies that except for the effect of tides, other factors, such as the winds and large-scale circulations, cannot be neglected in causing the interannual variations of the upwellings.

4. Sensitivity Experiments and Dynamic Analysis

According to the previous discussions, questions will be raised: Is there any other factor affecting the upwelling besides tides? Why is the effect of tidal mixing different on UWHI and USWHI? What are the dynamic

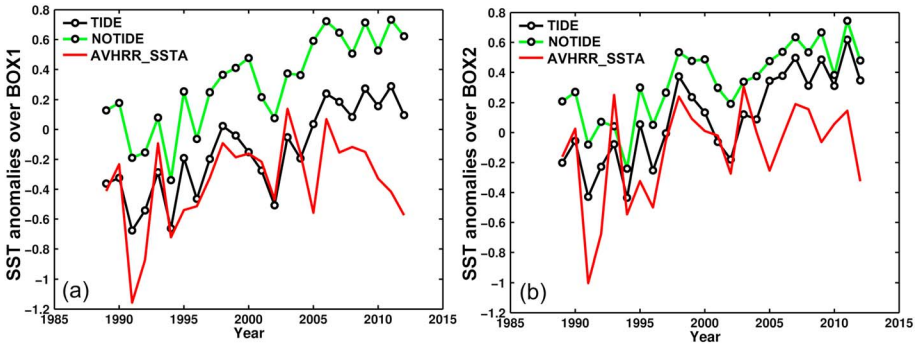

Figure 7. The time series of modeled SST anomalies in July (unit: °C) from inner-domain model outputs (green lines for NOTIDE; black lines for TIDE) and AVHRR data (red lines) averaged over (a) Box 1 and (b) Box 2, which are indicated in Figure 1b. SST = sea surface temperature; SSTA = SST anomaly; AVHRR = Advanced Very High Resolution Radiometer.

factors affecting the seasonal and interannual variations of UWHI and USWHI? To answer these questions, a set of sensitivity experiments is designed, as described in section 2.3.

Besides the sea temperature, the change of horizontal divergence of water column defined as follows is used to investigate the change of upwelling intensity:

$$Div = \frac{\partial uD}{\partial x} + \frac{\partial vD}{\partial y}. \tag{1}$$

We employ the following vertically integrated momentum equations (Mellor, 2004) for the dynamic analysis:

$$\begin{aligned} \frac{\partial uD}{\partial t} = &\underbrace{-\frac{\partial u^2 D}{\partial x} - \frac{\partial uvD}{\partial y}}_{AD} + \widetilde{F}_x + \underbrace{G_x}_{COR} + \underbrace{fvD}_{PBT} - gD\frac{\partial \eta}{\partial x} \\ &\underbrace{-\frac{gD}{\rho_0}\int_{-1}^{0}\int_{\sigma}^{0}\left[D\frac{\partial \rho'}{\partial x} - \frac{\partial D}{\partial x}\sigma'\frac{\partial \rho'}{\partial \sigma}\right]d\sigma' d\sigma}_{PBC} - \underbrace{wu(0)}_{WS} + \underbrace{wu(-1)}_{BOT}, \end{aligned} \tag{2}$$

and

$$\begin{aligned} \frac{\partial vD}{\partial t} = &\underbrace{-\frac{\partial v^2 D}{\partial y} - \frac{\partial uvD}{\partial x}}_{\mathrm{AD}} + \widetilde{F}_y + \underbrace{G_y}_{\mathrm{COR}} - \underbrace{fuD}_{\mathrm{PBT}} - gD\frac{\partial \eta}{\partial y} \\ &\underbrace{-\frac{gD}{\rho_0}\int_{-1}^{0}\int_{\sigma}^{0}\left[D\frac{\partial \rho'}{\partial y} - \frac{\partial D}{\partial y}\sigma'\frac{\partial \rho'}{\partial \sigma}\right]d\sigma' d\sigma}_{\mathrm{PBC}} - \underbrace{wv(0)}_{\mathrm{WS}} + \underbrace{wv(-1)}_{\mathrm{BOT}}, \end{aligned} \tag{3}$$

where x, y, and z are the conventional Cartesian coordinates; g is the sea level; $D = H + \eta$ is the total water depth, with $H(x, y)$ being the bottom topography and $\eta(x, y, t)$ the surface elevation; σ is the sigma coordinate ranging from $\sigma = 0$ at the sea surface to $\sigma = -1$ at the bottom; and ρ and ρ' are the density and density perturbation, respectively. Terms 1 to 6 on the right-hand side of equations (2) and (3) are referred to as nonlinear advection and diffusion (AD), Coriolis force (COR), barotropic pressure gradient (PBT), baroclinic pressure gradient (PBC), surface wind stress (WS), and bottom friction stress (BOT). Then the approximate divergence tendency equation can be obtained by $\left(\frac{\partial}{\partial x}\cdot(2) + \frac{\partial}{\partial y}\cdot(3)\right)$, which leads to

$$\begin{aligned} \frac{\partial Div}{\partial t} = &\underbrace{\left(\frac{\partial \mathrm{AD}_u}{\partial x} + \frac{\partial \mathrm{AD}_v}{\partial y}\right)}_{\mathrm{Tendency}} + \underbrace{f\varphi - \beta uD}_{\mathrm{DAD}} + \underbrace{\frac{\partial \mathrm{PBT}_u}{\partial x} + \frac{\partial \mathrm{PBT}_v}{\partial y}}_{\mathrm{DCOR}} + \underbrace{\frac{\partial \mathrm{PBC}_u}{\partial x} + \frac{\partial \mathrm{PBC}_v}{\partial y}}_{\mathrm{DPG}} \\ &+ \underbrace{\frac{\partial \mathrm{WS}_u}{\partial x} + \frac{\partial \mathrm{WS}_v}{\partial y}}_{\mathrm{DWS}} + \underbrace{\frac{\partial \mathrm{BOT}_u}{\partial x} + \frac{\partial \mathrm{BOT}_v}{\partial y}}_{\mathrm{DBOT}}), \end{aligned} \tag{4}$$

where ϕ is the vertical conservative vorticity and is defined as

$$\varphi = \frac{\partial vD}{\partial x} - \frac{\partial uD}{\partial y}. \tag{5}$$

According to equation (4), the tendency of divergence is caused by advection and diffusion (DAD), β effect and vertical vorticity of currents (DCOR), pressure gradient (DPG), wind stress (DWS), and bottom friction (DBOT). The DPG term consists of two parts: divergence tendency induced by barotropic pressure gradient and that induced by baroclinic pressure gradient, denoted as DPBT and DPBC, respectively. It should be noted that the DWS defined here is the "direct" local wind effect on the divergence tendency, while the "indirect" wind effect is included in the DPBT. The increase of divergence enhances upwelling through the Ekman pumping, while the decrease suppresses it.

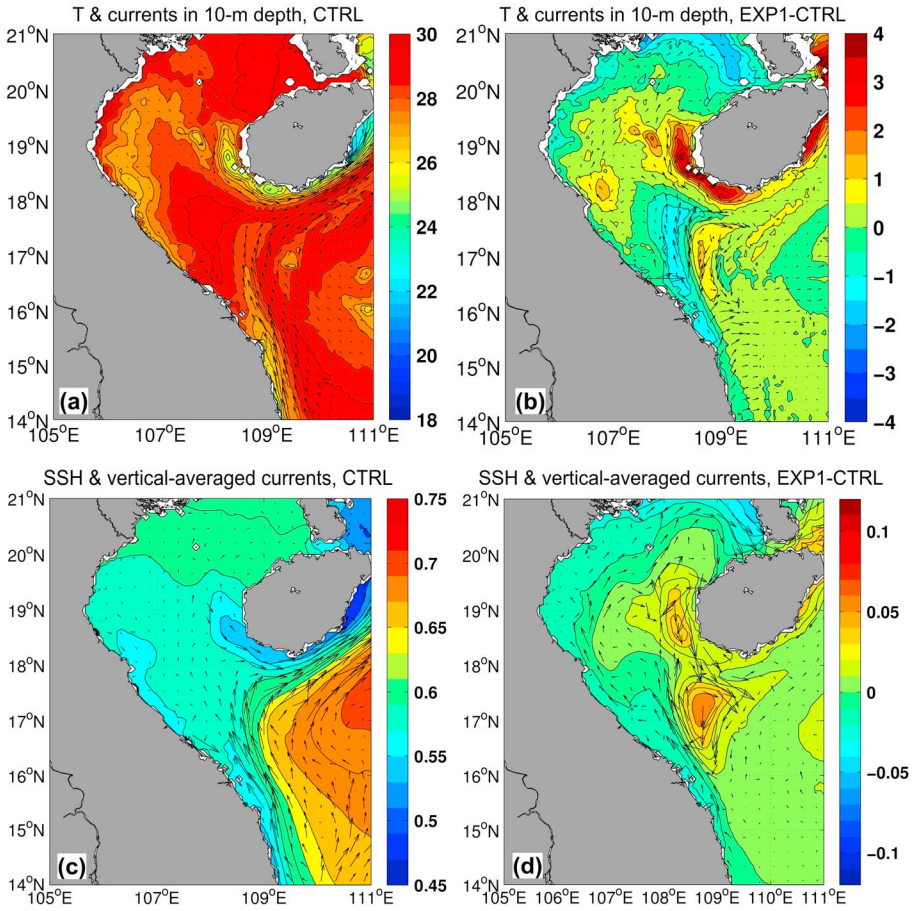

Figure 8. (top) The sea temperature (unit: °C) superimposed by currents in the 10-m depth and (bottom) the sea surface height (SSH; unit: m) superimposed by vertical-integrated currents for (a, c) CTRL and (b, d) EXP1-CTRL.

4.1. Joint Effect of Tidal Mixing and Stratification

The subsurface temperature and currents from sensitivity experiments are shown in Figure 8. The CTRL experiment, which includes the tidal effect, can reproduce the cooler sea surface water centers with lower SSH caused by divergence in the west and southwest off the Hainan Island (Figures 8a and 8c). Unlike the upwelling induced by winds in the eastern coast with cold sea surface water center in the near-shore region, the cooler sea surface centers of UWHI locate a little bit far away from the near-shore region. Moreover, EXP1 with tides excluded has anomalously warm subsurface water west and southwest off the Hainan Island compared to CTRL with tides included (Figure 8b), confirming that tidal effect is vital to the upwelling of these regions.

The effect of tides on the mixing can be estimated by the bottom mixing rate in the model. As shown in Figure 9a, inside the Beibu Gulf, large bottom mixing rates for CTRL locate mainly west and southwest off the Hainan Island as well as in the northern region of the Gulf where currents interact with steep bathymetry. Moreover, the bottom mixing rate, derived from the shear of currents in the bottom, is larger west off the island than southwest. When tides are excluded in the model, these large mixing rates are greatly reduced both west and southwest off the Hainan Island (Figure 9b), suggesting that tidal currents are crucial to the bottom mixing rate in these regions. In addition, high mixing rate centers are located in offshore regions, which is consistent with the offshore pattern of the cooler sea surface water centers shown in Figure 8a.

The spatially varying pattern of tidal mixing (shown in Figure 9a) together with the background stratification can change the circulation of the northwestern SCS, which can further affect the upwelling intensity. As shown in Figure 8c, it is clear that the main circulation of the northwestern SCS follows the isolines of SSH in July, which are parallel to the slope isobars of the continental shelf (Figure 1b). The inhomogenous

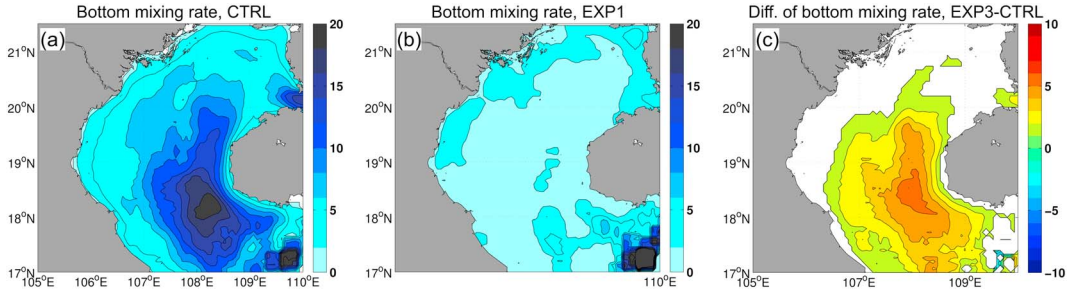

Figure 9. The vertical mixing rate (unit: 10^{-3} m^2/s) in the sea bottom layer for (a) CTRL and (b) EXP1 and (c) the differences of the vertical mixing rate (unit: 10^{-3} m^2/s) between EXP3 and CTRL.

mixing reductions can induce the inhomogenous temperature increase (density decrease) in summer when tides are absent as shown in Figures 8 and 9, which can force the anticyclonic circulation changes based on the geostrophic balance. As a result, two anomalous anticyclonic circulations are induced in the Beibu Gulf when tides are excluded (Figures 8b and 8d), which results in a northward shift of the western boundary currents of SCS (WBCSCS) along the eastern coast of Vietnam and southern coast of the Hainan Island. These anticyclonic circulation changes induce the convergence of sea water west and southwest off the Hainan Island, resulting in a significant increase of SSH (Figure 8d). Figure 10 further shows the relation between the upwelling and the main circulations. Similar to that in Figure 8a, there is a strong southward currents off the western coast of the Hainan Island as shown in Figure 10. The strong southward current is a little bit away from the coastal region, and the upwelling is intensified in the coastal region when tides are included (Figure 10a), whereas it is much closer to the coast and the downwelling is induced when tides are excluded (Figure 10b). These results imply that the spatially varying tidal mixing has a large impact on UWHI through changing the circulation.

The sea temperature, density, and mixing rate in section AB shown in Figures 11 and 12 give more information about the current-terrain interaction and the seasonal variations of the tidal mixing and UWHI. In the late winter (Figures 10a, 10e, 11a, and 11e), the temperature is well mixed and not stratified due to the strong northeast monsoon winds in the coastal region. As a result, the temperature profiles with and without tides are similar even though the mixing rate is larger near the western coast of the Hainan Island (near B) when tides are included. In the mid-spring (Figures 11b, 11f, 12a, and 12e), the stratification of temperature begins to establish due to the increasing surface heating and weaker wind stress with wind-induced mixing mainly being restricted in surface and subsurface. In summer (Figures 11c, 11g, 12c, and 12g), strong heating continues to stratify the sea water and strong tidal mixing in the steep-terrain regions west off the Hainan Island (Figure 12c) induces upwelling there (Figure 11c). As the autumn comes (Figures 11d, 11h, 12d, and 12h), enhanced wind-induced mixing destroys the stratification in the upper ocean and the effect of upwelling starts to disappear (Figure 11d). As shown in Figures 12i–12l, although the tidal mixing rate varies

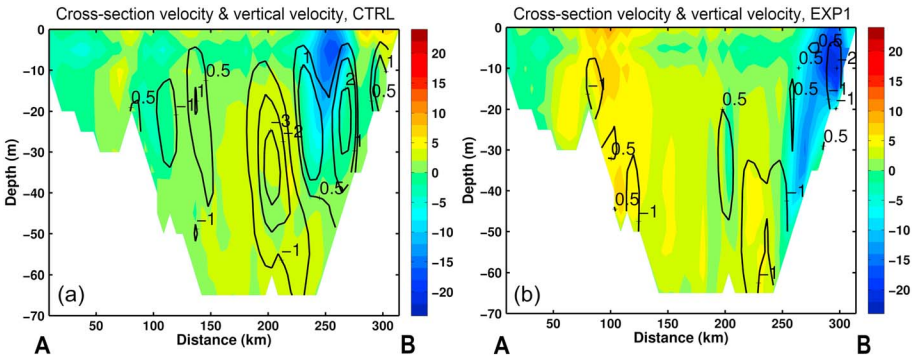

Figure 10. The cross-section velocity (colors, negative refers to the southward currents, while positive is northward currents, unit: cm/s) superimposed the vertical velocity (contours, unit: 10^{-5} m/s) along section AB for (a) CTRL and (b) EXP1 in July.

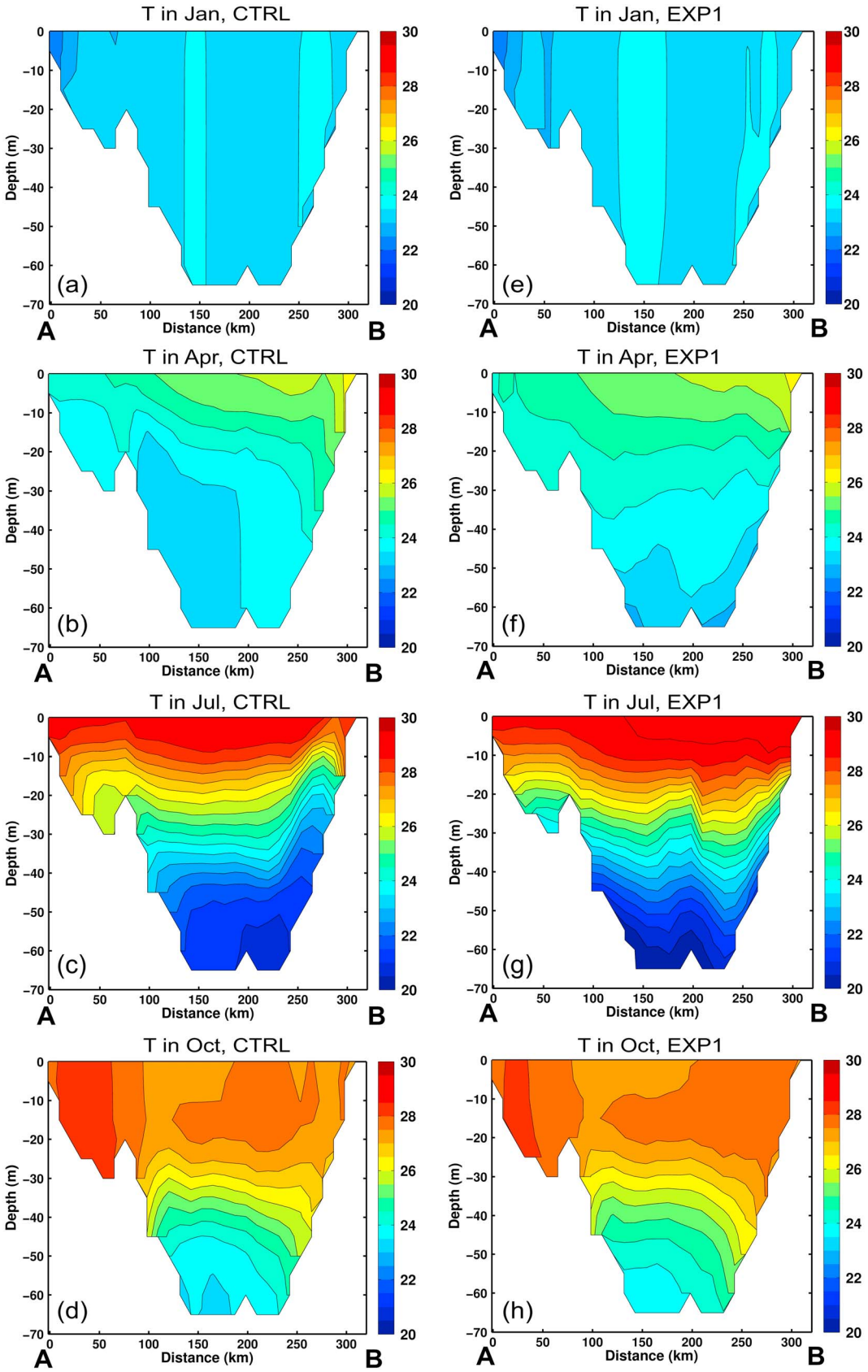

Figure 11. The sea temperature (unit: °C) along section AB in (a, e) January, (b, f) April, (c, g) July, and (d, h) October for (a–d) CTRL and (e–h) EXP1.

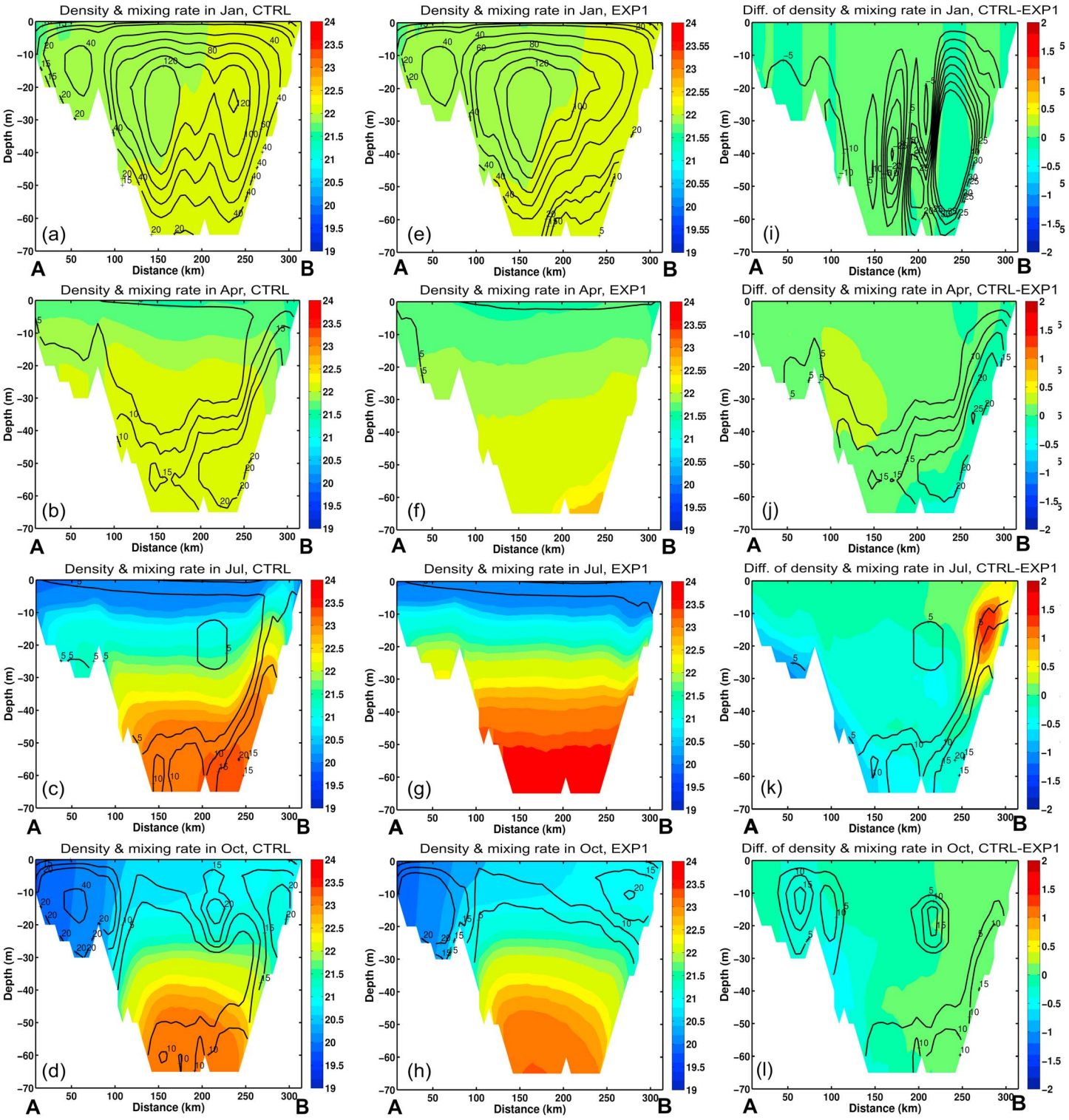

Figure 12. The sea density (colors, unit: 10^3 kg/m^3) superimposed by the vertical mixing rate (contours, unit: 10^{-3}m^2/s) along section AB in (a, e, i) January, (b, f, j) April, (c, g, k) July, and (d, h, l) October for (left) CTRL, (middle) EXP1, and (right) CTRL-EXP1.

seasonally in the open ocean, it has little change in the coastal region near the Hainan Island (location B) throughout the year. In the warm seasons, it is obvious that the tidal mixing rate is dominant in the total mixing rate in the subsurface and deeper ocean due to the weak wind-induced mixing rate (Figures 12c,

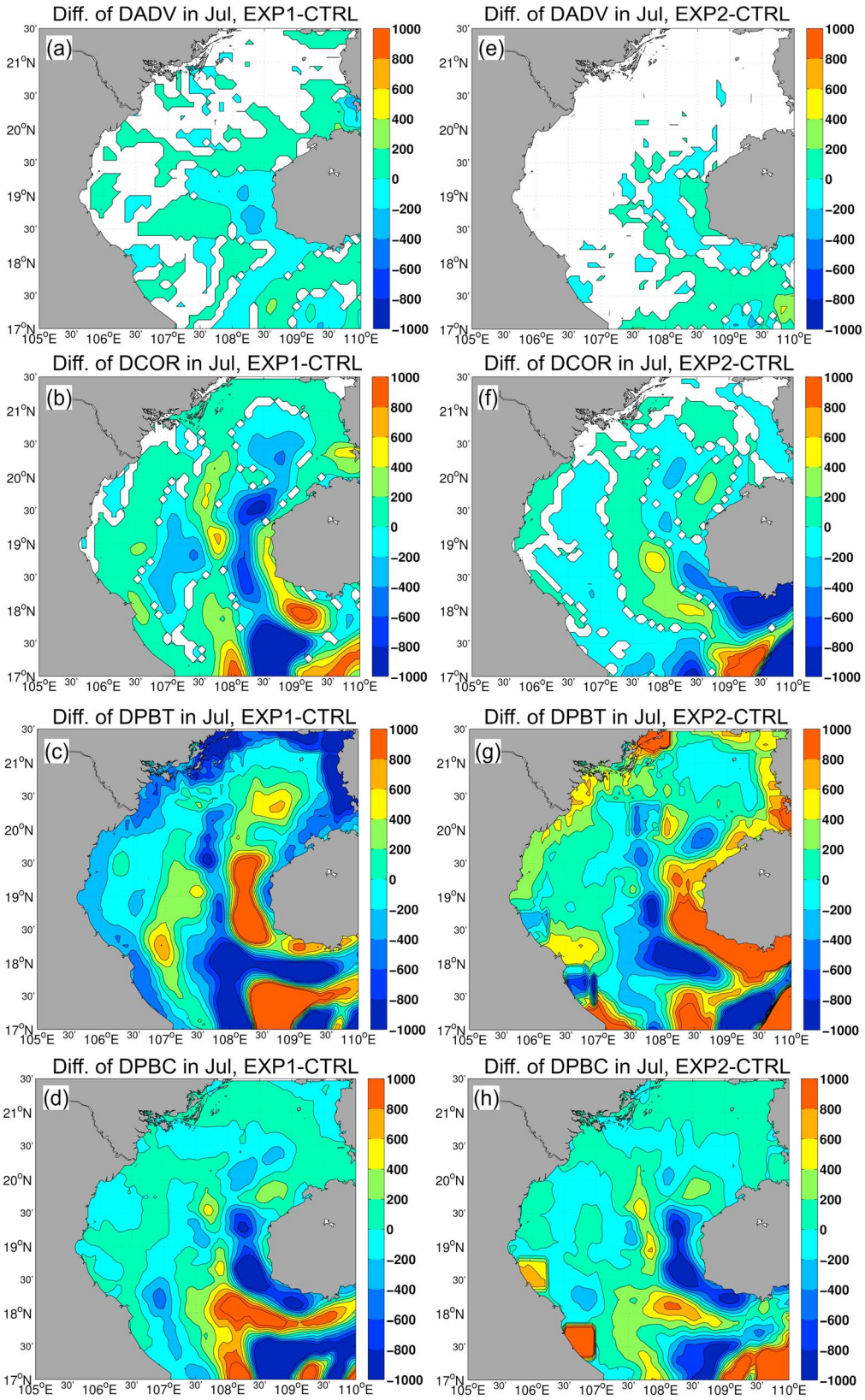

Figure 13. The differences of monthly-mean dynamic terms in the divergence tendency equation in July for (a, e) DAD, (b, f) DCOR, (c, g) DPBT, and (d, h) DPBC (unit: s^{-2}) between (left) EXP1 and CTRL (EXP1-CTRL) and between (right) EXP2 and CTRL (EXP2-CTRL).

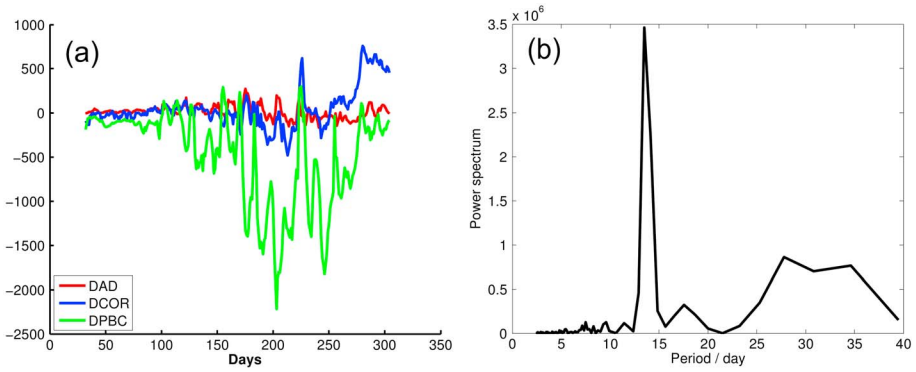

Figure 14. (a) The daily variations of dynamic term differences (@@DAD, DCOR, and DPBC, unit: s^{-2}) and (b) the power spectrum of variations of differences for DPBC in the divergence tendency equation averaged over Box 1 between EXP2 and CTRL (EXP2-CTRL; Day 1 refers to 1 January).

12g, and 12k); a density anomaly is seen over the shelf west off the Hainan Island (Figure 12k), which is associated with the inhomogenous distribution of tidal mixing between the open ocean and the coastal region and can cause strong horizontal baroclinic pressure gradients (PBC) in the steep terrain region west off the Hainan Island.

The differences of dynamic terms in the divergence tendency equation in July between EXP1 and CTRL are investigated and shown in Figure 13. DPBC, DCOR, and DAD induce convergence tendency (negative value indicates convergence or weakening of upwelling) west off the Hainan Island, while DPBC and DAD are the main sources of convergence tendency southwest off the Hainan Island (Figures 13a–13d). Here the change of DCOR refers to the impact of current changes on the divergence, which indicates that the convergence centers are mainly in the regions of the anticyclonic circulations (Figures 8d and 13b). In both west and southwest off the Hainan Island, the DPBC is the main force term for the convergence tendency. The mechanism associated with Figures 12 and 13 can be described as follows: In the cold seasons when the background stratification is weak (Figures 12i and 12l), the spatial inhomogenous tidal mixing cannot induce significant changes of density distribution; in the warm season when the background stratification is strong, the inhomogenous tidal mixing between the open ocean and the coastal region induces the inhomogenous changes of density in the region west off the Hainan Island (Figure 12k). These inhomogenous changes of density can further induce the changes of PBC and thus the changes of circulation, resulting in an increase of divergence and the generation of upwelling.

To further illustrate the effect of stratification on UWHI, the daily variations of the differences of dynamic terms in the divergence tendency equation averaged over Box 1 between EXP2 and CTRL from February to October are shown in Figure 14a. Compared to CTRL, EXP2 obtains negative changes of DAD, DCOR, and DPBC in the near-coast region of the Hainan Island (near location B) during late spring to the whole summer (120–270 days in Figure 14a); in the rest of the year when stratification is weak, there is no significant negative changes in these terms. In addition, the variations of the differences of these terms have a period of around 14 days, which is consistent with the period of spring-neap tides (the power spectrum of DPBC shown in Figure 14b). Therefore, these results confirm that the join effect of tidal mixing and stratification is crucial to the increase of divergence tendency and thus to the generation and seasonal variations of UWHI.

Similar results are obtained for USWHI (Figure 15). However, USWHI shows some obvious differences with UWHI in the relative importance of various factors influencing the generation and seasonal variations of the upwellings. First, the differences of temperature, mixing rate, SSH, and divergence tendency between EXP1 and CTRL for UWHI are larger than those for USWHI (Figures 8, 12c, 13, and 15c). Second, as shown in Figures 8d, 15c, and 15d, there is an offshore shift of northeastward WBCSCS (indicated by the lower density near location D) when tides are included. The offshore shift of WBCSCS when tides are included allows the cooler water (higher density) to uplift from the deeper ocean into the surface and subsurface southwest off the Hainan Island (near location D, shown in Figures 15a and 15c). This result is similar to the weakening of coastal main currents west off the Hainan Island caused by tides, which contributes to the strong upwelling there. However, the local tidal mixing is weaker southwest than west (Figures 12c and 15c), and thus, its

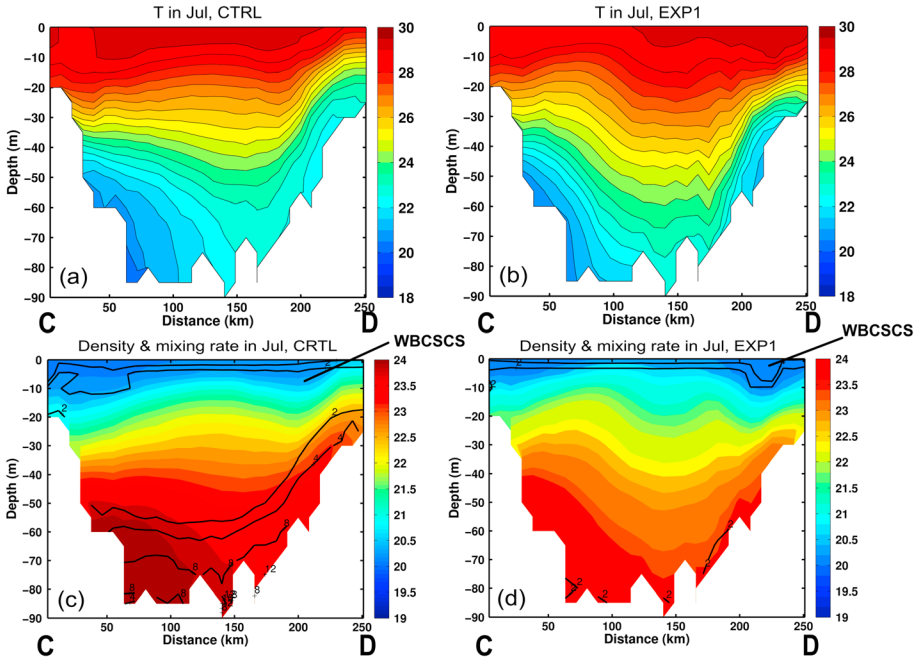

Figure 15. (a, b) The sea temperature (unit: °C) and (c, d) the sea density (unit: 10^3 kg/m^3) superimposed by the vertical mixing rate (contours, unit: 10^{-3}m^2/s) along section CD in July for (a, c) CTRL and (b, d) EXP1. WBCSCS = western boundary currents of South China Sea.

impacts on USWHI are much smaller. It implies that the change of WBCSCS path caused by tides is the main factor influencing USWHI, while the change of currents and locally vertical mixing induced by tides are both important to UWHI.

4.2. Factors Influencing the Interannual Variations of UWHI and USWHI

Although the changes of tides amplitudes are very small in the interannual scale, the effect of tidal mixing on upwelling and currents could be changed significantly due to nonlinear processes, which contributes to the interannual variations of UWHI and USWHI. For example, when changing the tidal forcing of 1998 to that of 2003 (EXP3), significant changes of the bottom mixing rate are found both west and southwest off the Hainan Island (Figures 2b and 9c), which results in the intensity changes of the upwellings there as indicated by the differences of temperature in the 10-m layer (Figure 16a), with the maximum changes of ~ — 1.5 °C west and ~ — 1.0 °C southwest off the Island. In addition to the tidal mixing, the variations of other factors can also contribute to the interannual variations of UWHI and USWHI, such as those of surface winds and the boundary currents (large-scale circulations) in the northwestern SCS. For instance, when changing the wind forcing

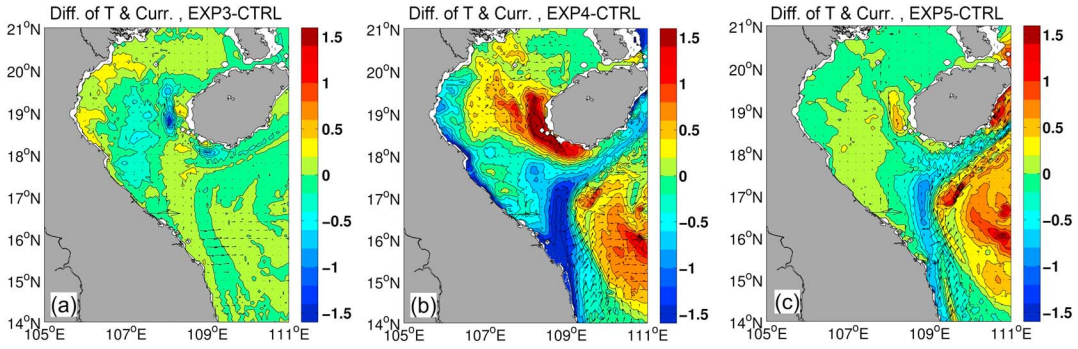

Figure 16. The differences of sea temperature (unit: °C) and currents in the 10-m depth in July between (a) EXP3 and CTRL; (b) EXP4 and CTRL; and (c) EXP5 and CTRL.

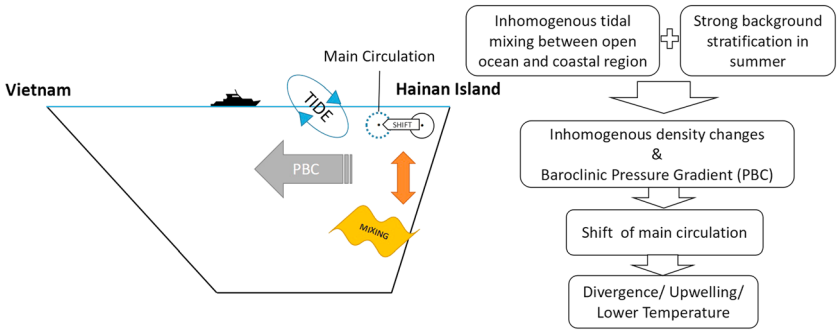

Figure 17. A schematic diagram illustrating the mechanisms of the upwelling west and southwest off the Hainan Island.

of climatology to that of 1998 (stronger along-shore wind forcing, EXP4), anomalously warm subsurface water is found west (with a maximum of ~1.7 °C) and southwest (with a maximum of ~1.2 °C) off the Hainan Island (Figure 16b); when changing the boundary conditions (large-scale circulations) of climatology to those of 1998 (EXP5), anomalously warm subsurface water is found west (with a maximum of ~0.7 °C) and southwest (with a maximum of ~0.3 °C) off the Hainan Island (Figure 16c). Obviously, it is the relative weak tidal mixing, enhanced along-shore winds, and strong boundary currents that result in the weakest UWHI and USWHI in 1998 as shown in Figure 2a, and the enhanced along-shore winds have the largest contribution.

5. Conclusion

Strong upwelling centers west and southwest off the Hainan Island can be detected by the satellite SST images during summer. A domain-nested high-resolution model POM is used to investigate the mechanisms of the upwelling generation and variations in seasonal and interannual time scales. The model is able to simulate the summer upwellings as well as their interannual variations. Although strong tidal mixing occurs throughout the year, significant cooler water can only be uplifted during the period when the background stratification is strong, that is, the late spring and summer, suggesting that the joint effect of the tidal mixing and background stratification is essential to the generation of the upwellings. The sensitivity experiments further confirm that the joint effect of tidal mixing and background stratification plays a key role in the upwelling generation through modulating the circulations in the northwestern SCS. The dynamic analysis reveals that with tides included, the baroclinic pressure gradient (DPBC) and the advection of currents (DAD) are the main drivers of the cold water uplifting both west and southwest off the Hainan Island, although the β effect and vertical vorticity of currents (DCOR) also play an important role comparable to DPBC and DAD for the upwelling west off the Hainan Island. The mechanism of the upwellings west and southwest off the Hainan Island is schematically illustrated in Figure 17.

The sensitivity experiments also reveal that the changes of the tidal mixing, the along-shore winds, and the boundary currents are the main causes of the interannual variations of the upwellings both west and southwest off the Hainan Island. In particular, it is the relative weak tidal mixing, enhanced along-shore winds, and strong boundary currents that result in the weakest upwellings both west and southwest of the Hainan Island in 1998, with the enhanced along-shore winds being the largest contributor. The connections between variations of the upwelling in the regions and large-scale climate variability are not discussed in this study, which will be our future work. In addition, the biases in the SST simulation in this study can be reduced through SST and sea level anomaly assimilation (Zheng et al., 2006, 2007), which will be our future work, too.

Acknowledgments
We are grateful to the freely available data as follows: sea surface temperature data provided by NASA/JPL, available at ftp://podaac.jpl.nasa.gov/pub/sea_surface_temperature/avhrr/pathfinder/data_v5/; the MODIS data provided by NASA, available at https://oceancolor.gsfc.nasa.gov/data/10.5067/AQUA/MODIS_OC.2014.0/; and SODA data, available at http://www.atmos.umd.edu/~ocean/index_files/soda3.3.1_mn_download.htm. This work was jointly supported by the Strategic Priority Research Program of the Chinese Academy of Sciences (Grant Nos. XDA19060503, XDA13030103), Innovation Research Group of National Natural Science Foundation of China (No. 41521005) National Natural Science Foundation of China (Grants Nos. 41776028 and 41676016), Science and Technology Program of Guangzhou, China (Grant No. 201607020043), and Science and Technology Planning Project of Guangdong Province, China (Grant No. 20150217). The authors gratefully acknowledge the use of the HPCC at the South China Sea Institute of Oceanology, Chinese Academy of Sciences. The views, opinions, and findings contained in this report are those of the authors and should not be construed as official NOAA or U.S. Government positions, policies, or decision.

References

Bakun, A., Field, D. B., Redondo-Rodriguez, A., & Weeks, S. J. (2010). Greenhouse gas, upwelling-favorable winds, and the future of coastal ocean upwelling ecosystems. *Global Change Biology*, *16*(4), 1213–1228. https://doi.org/10.1111/j.1365-2486.2009.02094.x

Bao, X., Hou, Y., Chen, C., Chen, F., & Shi, M. (2005). Analysis of characteristics and mechanism of current system on the west coast of Guangdong of China in summer. *Acta Oceanologica Sinica*, *24*, 1–9.

Blumberg, A. F., & Mellor, G. L. (1987). A description of a three-dimensional coastal ocean circulation model. In N. S. Heaps (Ed.), *Three-dimensional coastal ocean models* (pp. 1–16). Washington, DC: American Geophysical Union. https://doi.org/10.1029/CO004p0001

Carton, J. A., & Giese, B. S. (2008). A reanalysis of ocean climate using Simple Ocean Data Assimilation (SODA). *Monthly Weather Review*, *136*(8), 2999–3017. https://doi.org/10.1175/2007MWR1978.1

Chai, F., Xue, H., & Shi, M. (2001). Upwelling east of Hainan Island (in Chinese). In H. Xue, F. Chai, & J. Xu (Eds.), *Oceanography in China* (Vol. 13, pp. 129–137). Beijing: China Ocean Press.

Egbert, G. D., Bennett, A. F., & Foreman, M. G. G. (1994). TOPEX/Poseidon tides estimated using a global inverse model. *Journal of Geophysical Research*, *99*, 24,821–24,852. https://doi.org/10.1029/94JC01894

Ekman, V. W. (1905). On the influence of the Earth's rotation on ocean currents. *Arkiv för Matematik, Astronomi och Fysik*, *2*(11), 1–52.

Guan, B. X., & Chen, S. J. (1964). *Ocean current system in East China Sea and South China Sea* (in Chinese). Institute of Oceanology, Chinese Academy of Sciences: Qingdao.

Guo, F., Si, M. C., & Xia, Z. W. (1998). Two-dimension diagnose model to calculate upwelling on offshore of the east coast of Hainan Island (in Chinese). *Acta Oceanologica Sinica*, *20*, 109–116.

Jing, Z., Qi, Y., & Du, Y. (2011). Upwelling in the continental shelf of northern South China Sea associated with 1997–1998 El Niño. *Journal of Geophysical Research*, *116*, C02033. https://doi.org/10.1029/2010JC006598

Jing, Z., Qi, Y., Hua, Z., & Zhang, H. (2009). Numerical study on the summer upwelling system in the northern continental shelf of the South China Sea. *Continental Shelf Research*, *29*(2), 467–478. https://doi.org/10.1016/j.csr.2008.11.008

Kalnay, E., Kanamitsu, M., Kistler, R., Collins, W., Deaven, D., Gandin, L., et al. (1996). The NCEP/NCAR 40-year reanalysis project. *Bulletin of the American Meteorological Society*, *77*(3), 437–471. https://doi.org/10.1175/1520-0477(1996)077<0437: TNYRP>2.0.CO;2

Li, L. (1990). A study on the summer upwelling in the shelf waters west to Zhujiang River mouth (in Chinese). *Journal of Oceanography in Taiwan*, *9*, 338–346.

Li, Y., Peng, S., Yang, W., & Wang, D. (2012). Numerical simulation of the structure and variation of upwelling off the east coast of Hainan Island using QuikSCAT winds. *Chinese Journal of Oceanology and Limnology*, *30*(6), 1068–1081. https://doi.org/10.1007/s00343-012-1275-8

Locarnini, R. A., Mishonov, A. V., Antonov, J. I., Boyer, T. P., Garcia, H. E., Baranova, O. K., et al. (2013). World ocean atlas (2013), volume 1: Temperature ed S Levitus and A Mishonov vol 73 (Silver Spring, MD: Technical Ed NOAA Atlas NESDIS) (40 pp.).

Lü, X., Qiao, F., Wang, G., Xia, C., & Yuan, Y. (2008). Upwelling off the west coast of Hainan Island in summer: Its detection and mechanisms. *Geophysical Research Letters*, *35*, L02604. https://doi.org/10.1029/2007GL032440

Marks, K. M., & Smith, W. H. F. (2006). An evaluation of publicity available global bathymetry grids. *Marine Geophysical Researches*, *27*(1), 19–34. https://doi.org/10.1007/s11001-005-2095-4

Mellor, G. L. (2004). Users guide for a three-dimensional, primitive equation, numerical ocean model (June 2004 version), 53 pp., Prog. In Atmos. and Ocean. Sci, Princeton Univ., Princeton, NJ.

Mellor, G. L., & Yamada, T. (1982). Development of a turbulence closure model for geophysical fluid problems. *Reviews of Geophysics and Space Physics*, *20*(4), 851–875. https://doi.org/10.1029/RG020i004p00851

Menge, B., & Menge, D. (2013). Dynamics of coastal meta-ecosystems: The intermittent upwelling hypothesis and a test in rocky intertidal regions. *Ecological Monographs*, *83*(3), 283–310. https://doi.org/10.1890/12-1706.1

Niino, H., & Emery, O. (1961). Sediment of shallow portions of East China Sea and South China Sea. *Geological Society of America Bulletin*, *72*(5), 731–761. https://doi.org/10.1130/0016-7606(1961)72[731:SOSPOE]2.0.CO;2

Shi, M., Chen, C., Xu, Q., Lin, H., Liu, G., Wang, H., Wang, F., et al. (2002). The role of the Qiongzhou Strait in the seasonal variation of the South China Sea circulation. *Journal of Physical Oceanography*, *32*(1), 103–121. https://doi.org/10.1175/1520-0485(2002)032<0103: TROQSI>2.0.CO;2

Su, J., Xu, M., Pohlmann, T., Xu, D., & Wang, D.-R. (2013). A western boundary upwelling system response to recent climate variation (1960–2006). *Continental Shelf Research*, *57*, 3–9. https://doi.org/10.1016/j.csr.2012.05.010

Su, J. L., & Yuan, Y. (2005). Hydrology and circulation in Beibu Gulf. In *Hydrology of China seas* (pp. 285–296). Beijing: China Ocean Press.

Wang, C., Wang, W., Wang, D., & Wang, Q. (2006). Interannual variability of the South China Sea associated with El Niño. *Journal of Geophysical Research*, *111*, C03023. https://doi.org/10.1029/2005JC003333

Wang, D., Yang, Y., Wang, J., & Bai, X. (2016). A modeling study of the effects of river runoff, tides, and surface wind-wave mixing on the Eastern and Western Hainan upwelling systems of the South China Sea, China. *Ocean Dynamics*. https://doi.org/10.1007/s10236-015-0857-3

Wang, J. (1996). Global linear stability of the 2-D shallow water equations: An application of the distributive theorem of roots for polynomials on the unit circle. *Monthly Weather Review*, *24*(6), 1301–1310.

Wu, D., Wang, Y., Lin, X., & Yang, J. (2008). On the mechanism of the cyclonic circulation in the Gulf of Tonkin in the summer. *Journal of Geophysical Research*, *113*, C09029. https://doi.org/10.1029/2007JC004208

Xia, H., Li, S., & Shi, M. (2001). A 3-D numerical simulation of Zwinddriven currents in the Beibu Gulf (in Chinese with English abstract). *Acta Oceanologica Sinica*, *23*(6), 11–23.

Xie, S.-P., Hafner, J., Tanimoto, Y., Liu, W. T., Tokinaga, H., & Xu, H. (2002). Bathymetric effect on the winter sea surface temperature and climate of the Yellow and East China Seas. *Geophysical Research Letters*, *29*(24), 2228. https://doi.org/10.1029/2002GL015884

Yu, M. G., & Liu, J. F. (1993). The system and pattern of the South China Sea circulation (in Chinese with English abstract). *Ocean Predict*, *10*(2), 13–17.

Zeng, X., Belkin, I. M., Peng, S., & Li, Y. (2014). East Hainan upwelling fronts detected by remote sensing and modelled in summer. *International Journal of Remote Sensing*, *35*(11–12), 4441–4451. https://doi.org/10.1080/01431161.2014.916443

Zhang, Y., Dong, J., Ling, J., Wang, Y., & Zhang, S. (2010). Phytoplankton distribution and their relationship to environmental variables in Sanya Bay, South China Sea. *Scientia Marina*, *74*(4), 783–792. https://doi.org/10.3989/scimar.2010.74n4783

Zhang, Y. C., & Qian, Y. F. (1999). Numerical simulation of the regional ocean circulation in the coastal area of China. *Advances in Atmospheric Sciences*, *16*(3), 443–450.

Zheng, F., Zhu, J., & Zhang, R.-H. (2007). The impact of altimetry data on ENSO ensemble initializations and predictions. *Geophysical Research Letters*, *34*, L13611. https://doi.org/10.1029/2007GL030451

Zheng, F., Zhu, J., Zhang, R.-H., & Zhou, G.-Q. (2006). Ensemble hindcasts of SST anomalies in the tropical Pacific using an intermediate coupled model. *Geophysical Research Letters*, *33*, L19604. https://doi.org/10.1029/2006GL026994